Beam-Space MIMO Radar for Joint Communication and Sensing With OTFS Modulation

Saeid K. Dehkordi, *Graduate Student Member, IEEE*, Lorenzo Gaudio,
Mari Kobayashi, *Senior Member, IEEE*, Giuseppe Caire, *Fellow, IEEE*,
and Giulio Colavolpe, *Senior Member, IEEE*

Abstract—Motivated by automotive applications, we consider joint radar sensing and data communication for a system operating at millimeter wave (mmWave) frequency bands, where a Base Station (BS) is equipped with a co-located radar receiver and sends data using the Orthogonal Time Frequency Space (OTFS) modulation format. We consider two distinct modes of operation. In *Discovery* mode, a single common data stream is broadcast over a wide angular sector. The radar receiver must detect the presence of not yet acquired targets and performs coarse estimation of their parameters (angle of arrival, range, and velocity). In *Tracking* mode, the BS transmits multiple individual data streams to already acquired users via beamforming, while the radar receiver performs accurate estimation of the aforementioned parameters. Due to hardware complexity and power consumption constraints, we consider a hybrid digital-analog architecture where the number of RF chains and A/D converters is significantly smaller than the number of antenna array elements. In this case, a direct application of the conventional MIMO radar approach is not possible. Consequently, we advocate a *beam-space approach* where the vector observation at the radar receiver is obtained through a RF-domain beamforming matrix operating the dimensionality reduction from antennas to RF chains. Under this setup, we propose a likelihood function-based scheme to perform joint target detection and parameter estimation in Discovery, and high-resolution parameter estimation in Tracking mode, respectively. Our numerical results demonstrate that the proposed approach is able to reliably detect multiple targets while closely approaching the Cramér-Rao Lower Bound (CRLB) of the corresponding parameter estimation problem.

Index Terms—MIMO radar, joint sensing and communication, OTFS, beamforming design.

I. INTRODUCTION

IN mmWAVE communications, it is crucial to compensate the high isotropic path-loss with a highly directional beamforming (BF) gain [1]. This requires fast and accurate initial beam acquisition, which must be established before reliable data transmission can take place (see, e.g., [2], [3] and references therein). For mobile applications, e.g., a BS operating as a road-side infrastructure node and communicating with moving vehicles, beam acquisition for new not yet connected vehicles entering the cell is particularly challenging. Furthermore, beam tracking is necessary for the already connected users in order to follow their motion [4], [5], [6]. In this paper, we consider an enhanced BS, equipped with a co-located radar receiver. While transmitting a data modulated signal in the downlink, the BS uses the backscatter signals in order to detect unknown users and estimate parameters of already acquired users. We assume that the user terminals (i.e., targets) are large metal objects with a good radar cross-section such as vehicles [7], [8], [9]. As an extension of our previous works [10], this paper studies the joint target detection and parameter estimation problem at the enhanced BS using OTFS, a multi-carrier modulation proposed in [11] and already studied in different Multiple-Input Multiple-Output (MIMO) configurations (see, e.g., [12], [13]).

Motivated by the need for low-latency initial beam acquisition and accurate beam tracking mentioned above, we consider two distinct modes. In the first one, referred to as *Discovery* mode, a single OTFS modulated signal (e.g., some cell-dependent beacon/control signal) is broadcast over a wide angular sector and the goal of the radar receiver is to detect the presence of targets (vehicles) that are not yet acquired, as well as estimating their relevant parameters (angle of arrival, range, and velocity). In the second one, referred to as *Tracking* mode, the BS sends multiple individually beamformed OTFS modulated data streams to already acquired users, and the goal of the radar receiver is to provide high-resolution estimates of the users' parameters. Note that in the system studied in this paper the communication subsystem reduces to completely conventional OTFS with RF beamforming. The communication performance of such systems has been

Saeid K. Dehkordi and Giuseppe Caire are with the Faculty of Electrical Engineering and Computer Science, Technical University of Berlin, 10587 Berlin, Germany (e-mail: s.khalilidehkordi@tu-berlin.de; caire@tu-berlin.de).

Lorenzo Gaudio and Giulio Colavolpe are with the Department of Engineering and Architecture, University of Parma, 43124 Parma, Italy, and also with the CNIT Research Unit, 43124 Parma, Italy (e-mail: lorenzo.gaudio@studenti.unipr.it; giulio.colavolpe@unipr.it).

Mari Kobayashi was with the Department of Electrical Engineering, Technical University of Munich, 80333 Munich, Germany. She is with Apple Technology Engineering B.V. & Co. KG, 80335 Munich, Germany (e-mail: kobamari@gmail.com).

Color versions of one or more figures in this article are available at https://doi.org/10.1109/TWC.2023.3245207.

Digital Object Identifier 10.1109/TWC.2023.3245207

extensively studied in numerous works (e.g. [14]) and need not be repeated here. The "joint communication and sensing" aspect of our work consists precisely in considering the radar sensing performance of the two modes, namely, discovery and tracking, while leaving the communication system untouched. Hence, we focus only on the target detection and parameter estimation problems in the two modes of interest.

We further stress the fact that the two radar subsystem operation modes (discovery and tracking) are not necessarily related. From a holistic system design perspective, one would alternate the two phases, in analogy with currently deployed mmWave 5G systems, where beam sweeping for beam acquisition is periodically repeated at the beginning of some frame or super-frame structure. For example, the output of the radar detector in the discovery mode can be used to speed up the initial beam acquisition of new users entering the cell (e.g., see [15]), and the parameters estimated in tracking mode can be fed into suitable algorithms for beam tracking (e.g., see [4]). The exploitation of such radar sensing functions in specific communication systems is however beyond the scope of the present paper. A specific frame structure alternating between discovery and tracking modes (in correspondence with wide-angle beacon signaling and beamformed data transmission slots) is highly application-dependent and is intentionally left open in this work.

There are basically two ways to estimate the angular position of a target: either using a highly directional Tx/Rx beam [16] and scanning different angular "bins" in successive slots or exploring *simultaneously* the whole angle domain with a wide angle Tx beam and using an antenna array observation at the Rx side, exploiting some array processing technique for Angle of Arrival (AoA) estimation. The latter approach is usually referred to as MIMO radar (see, e.g., [17]). The advantage of MIMO radar is that the AoA estimation can be accomplished "off the grid" by some super-resolution estimation technique [18], and therefore does not suffer from the discretization error in the angle domain. On the other hand, wide-angle illumination and array reception do not provide directional BF gain, which may be a problem when the Signal-to-Noise Ratio (SNR) at the radar receiver is low. Furthermore, demodulating and sampling a large number of antennas tightly integrated in a monolithic structure is highly impractical in terms of chip area and power consumption/heat management, especially when the data signal has a large bandwidth as in mmWave applications. While this problem does not exist in standard automotive radar based on specifically designed waveforms such as Frequency Modulated Continuous Wave (FMCW), that are locally narrowband [16], it is definitely one of the major technological hurdles for digitally modulated waveforms at mmWave. Therefore, its solution represents a critical step in order to enable joint communication and sensing, which is recognized as an important trend in 6th generation wireless systems [19], [20].

To address this problem, this paper considers a novel MIMO radar approach in the *beam-space domain*, where the radar receiver employs a Hybrid Digital-Analog (HDA) architecture, widely proposed for mmWave frequency bands (see, e.g., [2], [21] and references therein). In this case, the number of Radio Frequency (RF) chains (N_{rf}), implementing demodulation from RF to baseband and A/D conversion, is much smaller than the number of antenna array elements (N_{a}), and the dimensionality reduction from the N_{a} antenna elements to

the N_{rf} antenna ports is operated by a *reduction matrix* implemented in the analog RF domain. The columns of the reduction matrix define the coefficients of N_{rf} RF beamforming vectors. The role of such beamformers is twofold. On the one hand, they aim to "cover" sufficiently well the desired AoA domain. On the other hand, they should provide sufficient BF gain in order to achieve a good operating SNR of the radar receiver. The main contributions of this paper are summarized as follows:

1) We propose the use of multi-block processing with a randomized ensemble of carefully designed reduction matrices across the blocks to exploit the sparsity of mmWave channels in the beam-space domain. We demonstrate the superiority of the proposed BF codebook with respect to baseline choices, in particular, when the reduction matrices are constructed from Discrete Fourier Transform (DFT) beamforming vectors or from antenna selection.

2) For Discovery mode, we propose a sequential target detection, parameter estimation, and Successive Interference Cancellation (SIC) that at each detection step performs a likelihood ratio threshold test. SIC is used to avoid the masking effect of strong targets on weaker targets located at different ranges from the BS and not sufficiently separated in the Doppler-delay-AoA domain (near-far effect). The proposed scheme achieves multiple target detection over a relatively wide Field of View (FoV) and ranges comparable to Short/Medium range automotive radar systems [22], [23]. Furthermore, the range can be extended by increasing the number of processed blocks.

3) For Tracking mode, we propose a Maximum Likelihood (ML)-based scheme providing high-resolution (off-grid) estimation of AoA, delay, and Doppler parameters for multiple targets. We demonstrate through simulations that the parameter estimation performance approaches very closely the CRLB when the receiver SNR is not too small. In this mode, since the already acquired targets are individually illuminated by highly directive (narrow) beams, we obtain good parameter estimation accuracy for ranges comparable to Medium/Long range automotive radars [22].

The rest of the paper is organized as follows. In Section II we define the system model and review OTFS modulation introducing the necessary notations. In Section III we present the design of the proposed beamforming codebook for multi-block detection/estimation in the beam-space domain. Section IV discusses the details of the target detection and parameter estimation schemes. Section V presents simulation results and comparisons to alternative and more conventional MIMO radar schemes. Finally, Section VI provides our concluding remarks. The details of the BF design algorithm are presented in Appendix A and the method to calculate the adaptive threshold for the target detection scheme is given in Appendix B. We adopt the following notations. $(\cdot)^{\mathsf{T}}$ denotes the transpose operation. $(\cdot)^{\mathsf{H}}$ denotes the Hermitian (conjugate and transpose) operation. $|x|$ denotes the absolute value of x if $x \in \mathbb{R}$ while $|\mathscr{X}|$ denotes the cardinality of a set $\mathscr{X}$. $\|\mathbf{x}\|$ denotes the ℓ_2-norm of a complex or real vector $\mathbf{x}$. $\mathbf{I}_m$ denotes the $m \times m$ identity matrix. We let $[n] = \{1, \ldots, n\}$ and $[0 : n] = \{0, 1, \ldots, n\}$ for a positive integer n.

II. System Model

A. Backscatter Channel Model

We consider a system operating over a channel with carrier frequency f_c and bandwidth W sufficiently smaller than f_c, such that the narrowband array response assumption holds [24], [25].[1] We consider a BS transmitter equipped with $N_{\rm rf}$ Tx RF chains driving an antenna array with $N_{\rm a}$ elements, and a radar receiver co-located with the BS. For simplicity of exposition, we assume that the Tx array and the Rx radar array coincide and that the Tx and Rx signals are separated by some full-duplex processing.[2] However, all our results can be easily generalized to the case where the two arrays are different and sufficiently spatially separated such that the Tx signal does not saturate the radar Rx front-end.

We consider a point target model, such that each target is characterized by its Line-of-Sight (LoS) path only. This model is widely used in the literature (e.g., see [29], [30], [31]) and in our case it can be justified by our motivating scenario of a BS operating as road-side infrastructure node and communicating with moving vehicles on the road.

By letting $\phi \in [-\frac{\pi}{2}, \frac{\pi}{2}]$ denote the steering angle and considering a Uniform Linear Array (ULA) with $\lambda/2$ inter-element antenna spacings, the Tx/Rx array response is given by $\mathbf{a}(\phi) = (a_1(\phi), \ldots, a_{N_a}(\phi))^{\mathsf{T}} \in \mathbb{C}^{N_a}$, where

$$a_n(\phi) = e^{j(n-1)\pi \sin(\phi)}, \quad n = 1, \ldots, N_a. \tag{1}$$

Since this paper focuses on the radar processing, we consider the channel model for the backscatter signal. For the case of P targets, this is given by the superposition of P rank-1 channel matrices, each of which corresponds to the LoS propagation from the Tx array to each target and back to the radar Rx array along the same LoS path. This results in the $N_{\rm a} \times N_{\rm a}$ time-varying MIMO channel with matrix impulse response given by [32]

$$\mathbf{H}(t, \tau) = \sum_{p=0}^{P-1} \rho_p \mathbf{a}(\phi_p) \mathbf{a}^{\mathsf{H}}(\phi_p) \delta(\tau - \tau_p) e^{j2\pi \nu_p t}, \tag{2}$$

where for each target p, ρ_p is a complex channel gain including the LoS pathloss and the radar cross-section coefficient, $\nu_p = \frac{2v_p f_c}{c}$ is the round-trip Doppler shift, $\tau_p = \frac{2r_p}{c}$ is the round-trip delay (time of flight), and ϕ_p denotes the AoA.[3] We assume that the channel parameters $\{\rho_p, \phi_p, \nu_p, \tau_p\}_{p=1}^{P}$ remain constant over the coherence processing interval of B time-frequency blocks, where each time-frequency block consists of a frame of (roughly) $WT_{\rm frame}$ signal dimensions, with $T_{\rm frame}$ denoting the frame duration.

B. OTFS Modulation

We consider the OTFS modulation format as it is known to be robust to high Doppler shifts and efficient in the presence

of sparse channels in the Doppler-delay domain [10]. OTFS is a multicarrier scheme with M subcarriers with separation Δf, such that the total bandwidth is $W = M\Delta f$. We let T denote the symbol time and N denote the number of OTFS symbols per frame, yielding a frame duration of $T_{\rm frame} = NT$. We also consider $T\Delta f = 1$, which is typical in most OTFS literature [10], [11], [33]. Let $N_{\rm s}$ denotes the number of data streams per frame to be sent by the BS, where $N_{\rm s} = 1$ corresponds to the broadcasting of a single data stream (Discovery mode) and $1 < N_{\rm s} \leq N_{\rm rf}$ corresponds to the transmission of $N_{\rm s}$ individual users' data streams (Tracking mode).

In what follows, we derive the relation between the block of data symbols and the signal at the radar receiver. Since OTFS is a linear modulation and the propagation channel is a linear (time-varying) system, this relation will be a linear mapping. For simplicity of exposition, we focus on a generic time-frequency block of NM symbols and neglect the block index. Section IV will consider the received signal across B blocks explicitly.

Following the standard derivation of the input-output relation of OTFS (see, e.g., [10], [11]), the $N_{\rm s}$-dimensional data symbol vectors $\{\mathbf{x}_{k,l} \in \mathbb{C}^{N_{\rm s} \times 1} : k \in [0 : N - 1], l \in [0 : M - 1]\}$, belonging to some suitable QAM constellation, are arranged in an $N \times M$ two-dimensional grid $\Gamma = \left\{ \left(\frac{k}{NT}, \frac{l}{M\Delta f} \right), k \in [0 : N - 1], l \in [0 : M - 1] \right\}$, referred to as the *Doppler-delay domain*. We can visualize $\{\mathbf{x}_{k,l}\}$ as a $N \times M \times N_{\rm s}$ three-dimensional block of data, where each horizontal layer of dimensions $N \times M$ represents one data stream. The Tx applies the Inverse Symplectic Finite Fourier Transform (ISFFT) layer by layer, converting the Doppler-delay domain data block $\{\mathbf{x}_{k,l}\}$ into the corresponding time-frequency data block $\{\mathbf{X}_{n,m}\}$, defined by

$$\mathbf{X}_{n,m} = \sum_{k=0}^{N-1} \sum_{l=0}^{M-1} \mathbf{x}_{k,l} e^{j2\pi \left(\frac{nk}{N} - \frac{ml}{M} \right)}, \tag{3}$$

for $n \in [0 : N - 1]$, $m \in [0 : M - 1]$. The symbols across time-frequency and data stream dimensions are uncorrelated, and we assume the average Tx power normalization

$$\mathbb{E}[\mathbf{X}_{n,m} \mathbf{X}_{n,m}^{\mathsf{H}}] = \frac{P_{\rm avg}}{N_{\rm s}} \mathbf{I}_{N_{\rm s}}, \quad \forall (n, m).$$

Then, the Tx generates the $N_{\rm s}$-dimensional continuous-time signal

$$\mathbf{s}(t) = \sum_{n=0}^{N-1} \sum_{m=0}^{M-1} \mathbf{X}_{n,m} g_{\rm tx}(t - nT) e^{j2\pi m\Delta f(t - nT)}. \tag{4}$$

For mmWave multiuser MIMO applications, different HDA architectures have been considered in the literature to handle the fact that the number $N_{\rm rf}$ of RF chains is generally significantly smaller than the number $N_{\rm a}$ of antenna array elements (e.g., [2], [34]). Letting $\mathbf{F} \in \mathbb{C}^{N_{\rm a} \times N_{\rm s}}$ and $\mathbf{U} \in \mathbb{C}^{N_{\rm a} \times N_{\rm rf}}$ denote the Tx and the Rx BF matrices, respectively, from (4) and (2), the $N_{\rm rf}$-dimensional continuous-time received signal

---

[1] In particular, this means that the baseband array response vector is essentially invariant with frequency in the interval $[-W/2, W/2]$.

[2] Full-duplex operations can be achieved with sufficient isolation between the transmitter and the (radar) detector and possibly interference analog pre-cancellation in order to prevent the (radar) detector saturation [26], [27], [28].

[3] In the expressions of ν_p and τ_p, c denotes the light speed, v_p is the velocity component of the p-th target in the radial direction with respect to the radar receiver, and r_p is the distance between the p-th target and the radar receiver.

at the radar Rx is obtained as[4]

$$\mathbf{r}(t) = \sum_{p=0}^{P-1} \rho_p \mathbf{U}^{\mathsf{H}} \mathbf{a}(\phi_p) \mathbf{a}^{\mathsf{H}}(\phi_p) \mathbf{F} \mathbf{s}(t - \tau_p) e^{j2\pi\nu_p t}. \quad (5)$$

The output of the Rx filter-bank adopting a generic receive shaping pulse $g_{\mathrm{rx}}(t)$ is given by (6), shown at the bottom of the page.

By sampling at $t = nT$ and $f = m\Delta f$, we obtain

$$\begin{aligned}
\mathbf{Y}_{n,m} &= \mathbf{Y}(t,f)|_{t=nT}^{f=m\Delta f} \\
&= \sum_{n'=0}^{N-1} \sum_{m'=0}^{M-1} \mathbf{H}_{n,n',m,m'} \mathbf{X}_{n',m'}, \quad (7)
\end{aligned}$$

where $\mathbf{H}_{n,n',m,m'}$ is given by (8), shown at the bottom of the page, and where we defined the cross ambiguity function $C_{u,v}(\tau,\nu) \triangleq \int_{-\infty}^{\infty} u(s)v^*(s-\tau)e^{-j2\pi\nu s}ds$ as in [35], let $h_p \triangleq \rho_p e^{j2\pi\nu_p\tau_p}$, and used the fact that $e^{-j2\pi mn'\Delta fT} = 1$, $\forall n', m$, under the hypothesis $T\Delta f = 1$. Finally, the received signal in the Doppler-delay domain is obtained by the application of the Symplectic Finite Fourier Transform (SFFT)

$$\mathbf{y}_{k,l} = \frac{1}{NM} \sum_{n,m} \mathbf{Y}_{n,m} e^{j2\pi\left(\frac{ml}{M} - \frac{nk}{N}\right)}. \quad (9)$$

In order to express (9) in a more explicit and useful form, we defined the general Doppler-delay crosstalk coefficient as given by (10), shown at the bottom of the page.

Then, using (7), (8), with (10), in (9), the signal component of the channel output at a given Doppler-delay pair k, l can be written as

$$\begin{aligned}
\mathbf{y}_{k,l} = \sum_{p=0}^{P-1} h_p \mathbf{U}^{\mathsf{H}} \mathbf{a}(\phi_p) \mathbf{a}^{\mathsf{H}}(\phi_p) \\
\times \mathbf{F} \sum_{k',l'} \Psi_{k,k',l,l'}(\nu_p, \tau_p) \mathbf{x}_{k',l'}. \quad (11)
\end{aligned}$$

In Discovery mode, the BS sends a single data stream ($N_{\mathrm{s}} = 1$) through a beamforming vector (i.e., $\mathbf{F} = [\mathbf{f}]$ is formed by a single column). The beamforming vector $\mathbf{f}$ is designed to

uniformly cover a given wide angular sector as the BS has no a priori knowledge of the location of the targets. In Tracking mode, the BS sends $N_{\mathrm{s}} = P \geq 1$ data streams through a beamforming matrix $\mathbf{F} = [\mathbf{f}_1, \ldots, \mathbf{f}_{N_{\mathrm{s}}}]$ where $\mathbf{f}_q$ denotes the q-th column of $\mathbf{F}$ associated to the q-th data stream. Appendix A presents the general method used in this work to design the Tx beamforming vectors $\mathbf{f}$ and the columns of $\mathbf{U}$.

We remark that (11) corresponds to a single-input (for $N_{\mathrm{s}} = 1$) or multiple input (for $N_{\mathrm{s}} = P > 1$) multiple-output channel with Inter-Symbol Interference (ISI), where the ISI occurs in the Doppler-delay domain.

III. BEAM-SPACE MIMO RADAR WITH MULTIPLE BLOCK RECEPTION

The fact that the number of RF chains N_{rf} is typically much smaller than the number of array antenna elements N_{a} yields the following fundamental problem: if the columns of the reduction matrix $\mathbf{U}$ correspond to narrow beams with a high BF gain, the AoA domain is not well explored (e.g., some targets might be missed). In contrast, if the columns of $\mathbf{U}$ correspond to wide angle beamforming patterns, the SNR at each receiver RF chain may be too low and the spatial resolution of each observation may be too coarse.

In order to circumvent this problem, we consider the joint processing of B consecutive blocks, where the reduction matrix varies from one block to another (we let $\mathbf{U}_b$ denote the reduction matrix in block $b \in [B]$). The idea is that while each reduction matrix consists of a set of narrow beams, the ensemble of B blocks is able to explore the FoV of interest without "holes". At each block b, we obtain an N_{rf}-dimensional observation, where each dimension corresponds to a beam pattern defined by a column of $\mathbf{U}_b$. Hence, we refer to this approach as *beam-space* MIMO radar.

We consider a BF codebook formed by a set of flat-top beams to span the required FoV, designed to provide sufficiently large BF gain (and therefore maintain a good receiver SNR) over a given angular span as compared to *sharp* "Fourier" beams (i.e., beamforming vectors obtained from the columns of a $N_{\mathrm{a}} \times N_{\mathrm{a}}$ DFT matrix). Let $\Omega = [\theta_{\min}, \theta_{\max}]$ denote the FoV and, for given step $\Delta\theta$, we divide $|\Omega| \triangleq |\theta_{\max} - \theta_{\min}|$ into an integer number $\frac{|\Omega|}{\Delta\theta}$ of intervals of size $\Delta\theta$. Each interval is further partitioned into an integer number $\frac{\Delta\theta}{\delta\theta}$

$$\begin{aligned}
\mathbf{Y}(t,f) &= \int \mathbf{r}(t') g_{\mathrm{rx}}^*(t'-t) e^{-j2\pi ft'} dt' = \int_{t'} g_{\mathrm{rx}}^*(t'-t) \sum_{p=0}^{P-1} \rho_p \mathbf{U}^{\mathsf{H}} \mathbf{a}(\phi_p) \mathbf{a}^{\mathsf{H}}(\phi_p) \mathbf{F} \mathbf{s}(t'-\tau_p) e^{j2\pi\nu_p t'} e^{-j2\pi ft'} dt' \\
&= \sum_{p,n',m'} \rho_p \mathbf{U}^{\mathsf{H}} \mathbf{a}(\phi_p) \mathbf{a}^{\mathsf{H}}(\phi_p) \mathbf{F} \mathbf{X}_{n',m'} \int_{t'} g_{\mathrm{rx}}^*(t'-t) g_{\mathrm{tx}}(t'-\tau_p - n'T) e^{j2\pi m'\Delta f(t'-\tau_p - n'T)} e^{j2\pi(\nu_p - f)t'} dt' \quad (6)
\end{aligned}$$

$$\mathbf{H}_{n,n',m,m'} = \sum_{p=0}^{P-1} h_p \mathbf{U}^{\mathsf{H}} \mathbf{a}(\phi_p) \mathbf{a}^{\mathsf{H}}(\phi_p) \mathbf{F} C_{g_{\mathrm{tx}},g_{\mathrm{rx}}}((n-n')T - \tau_p, (m-m')\Delta f - \nu_p) e^{j2\pi n'T\nu_p} e^{-j2\pi m\Delta f\tau_p} \quad (8)$$

$$\Psi_{k,k',l,l'}(\nu,\tau) \triangleq \sum_{n,n',m,m'} \frac{C_{g_{\mathrm{rx}},g_{\mathrm{tx}}}((n-n')T - \tau, (m-m')\Delta f - \nu)}{NM} e^{j2\pi n'T\nu} e^{-j2\pi m\Delta f\tau} e^{j2\pi\left(\frac{n'k'}{N} - \frac{m'l'}{M}\right)} e^{-j2\pi\left(\frac{nk}{N} - \frac{ml}{M}\right)} \quad (10)$$
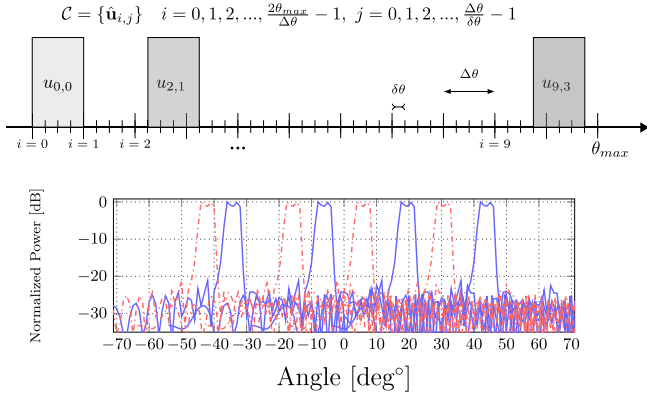
Fig. 1. (Top) Illustrative description of the atoms of the BF codebook. Without loss of generality, we assume a symmetric FoV covering $[-\theta_{\max}, \theta_{\max}]$. (Bottom) An example with $N_{\mathrm{rf}} = 4$ beams per block for $B = 2$ consecutive blocks (corresponding to the different colors), and a total of $N_{\mathrm{rf}}B = 8$ explored directions.

of subintervals of size $\delta\theta$. We let $\mathcal{C} := \{\widehat{\mathbf{u}}_{i,j} , i \in [0 : \frac{|\Omega|}{\Delta\theta} - 1], j \in [0 : \frac{\Delta\theta}{\delta\theta} - 1]\}$ denote a BF codebook, where each atom $\widehat{\mathbf{u}}_{i,j} \in \mathbb{C}^{N_{\mathrm{a}} \times 1}$ is a direction-shifted version of the fundamental flat-top beam $\widehat{\mathbf{u}}_{0,0}$ of width $\Delta\theta$ (designed using the method in Appendix A), with beam center direction given by $\theta_{\min} + i\Delta\theta + j\delta\theta$. The parameters $\Delta\theta$ and $\delta\theta$ are selected to seek a good trade-off between BF gain, angle coverage, and complexity of the beamforming codebook. We have constructed pseudo-random sequences of B reduction matrices such that at every block b, $\mathbf{U}_b$ consists of "non-overlapping" atoms from $\mathcal{C}$, (i.e., such that any two $n \neq n'$ columns of $\mathbf{U}_b$ satisfy $\mathbf{u}_{b,n}^{\mathsf{H}}\mathbf{u}_{b,n'} \approx 0$), and over the B blocks the union of the covered angular span is maximal. An example of such *multi-directional* beam patterns is illustrated in Fig. 1.

Extensive system simulations show that the system performance strongly depends on B for given N_{rf} and N_{a} but, for relatively large B, it is almost independent on the specific pseudo-random choice of the matrices $\{\mathbf{U}_b\}$ constructed according to the above principle.

Remark 1: An alternative to the use of directive beams in the HDA set-up discussed above consists of directly sampling N_{rf} antennas per block. We refer to this as the Antenna Selection *scheme, where the dictionary $\mathscr{C}$ is formed by the columns of an $N_{\mathrm{a}} \times N_{\mathrm{a}}$ identity matrix such that, at each block $b \in [B]$, each column of $\mathbf{U}_b$ consists of zeros except a single one corresponding to the antenna port being sampled. Another alternative for beam-space MIMO radar consists of using a grid of DFT beams, i.e., the dictionary $\mathscr{C}$ is formed by the columns of a $N_{\mathrm{a}} \times N_{\mathrm{a}}$ unitary DFT matrix. In Section IV-C, Fig. 2, a comparison between these alternatives in terms of the achieved CRLB for parameter estimation will be provided. We will show that antenna selection and the DFT dictionaries achieve generally worse performance than the proposed one for two opposite reasons: antenna selection provides good angle exploration but very low SNR at each sampled antenna port. The DFT dictionary provides very high BF gains but too limited angular support.* ◇

IV. JOINT DETECTION AND PARAMETERS ESTIMATION

We denote the true value of the parameters as $\mathring{\boldsymbol{\theta}} = \{\mathring{h}_p, \mathring{\nu}_p, \mathring{\tau}_p, \mathring{\phi}_p\}$ and use $\boldsymbol{\theta} = \{h_p, \nu_p, \tau_p, \phi_p\}$ to denote the

arguments of the likelihood function. We shall write the received signal expression (11) in a compact form by blocking the NM Doppler-delay signal components into $NM \times 1$ vectors. In order to avoid notation ambiguity, we use underline to denote blocked quantities. For each $b \in [B]$, we define the effective channel matrix of dimension $N_{\mathrm{rf}}NM \times N_{\mathrm{s}}NM$ as

$$\underline{\mathbf{G}}_b(\nu, \tau, \phi) \triangleq \left(\mathbf{U}_b^{\mathsf{H}}\mathbf{a}(\phi)\,\mathbf{a}^{\mathsf{H}}(\phi)\mathbf{F}\right) \otimes \mathbf{\Psi}(\nu, \tau), \quad (12)$$

where $\mathbf{\Psi}(\nu, \tau)$ is defined such that $[\mathbf{\Psi}(\nu, \tau)]_{kM+l,k'M+l'} = \Psi_{k,k',l,l'}(\nu, \tau)$ for $k, k' \in [0 : N-1]$ and $l, l' \in [0 : M-1]$, where $\Psi_{k,k',l,l'}(\nu, \tau)$ is defined in (10), and $\otimes$ is the Kronecker product. In (12), $\mathbf{F}$ is formed by a single column (Discovery mode with $N_{\mathrm{s}} = 1$) or multiple columns (Tracking mode with $N_{\mathrm{s}} = P$). Thus, by stacking the $N \times M \times N_{\mathrm{s}}$ OTFS symbol block into a $N_{\mathrm{s}}NM$-dimensional vector $\underline{\mathbf{x}}_b$ and defining the blocked output vector $\underline{\mathbf{y}}_b$ of dimension $N_{\mathrm{rf}}NM \times 1$, the received signal takes on the form

$$\underline{\mathbf{y}}_b = \left(\sum_{p=0}^{P-1} \mathring{h}_p \underline{\mathbf{G}}_b(\mathring{\nu}_p, \mathring{\tau}_p, \mathring{\phi}_p)\right)\underline{\mathbf{x}}_b + \underline{\mathbf{w}}_b, \quad b \in [B], \quad (13)$$

where $\underline{\mathbf{w}}_b$ denotes the additive white Gaussian noise (AWGN) vector with independent and identically distributed entries of zero mean and variance σ_w^2.

A. Target Detection and Parameter Estimation in Discovery Mode

In Discovery mode, the unknown number P of targets are simultaneously illuminated by a single wide FoV beacon signal. In this case, a near target may "mask" the presence of a far target with similar AoA. Hence, we propose to detect the targets sequentially and, after a target is detected and its parameters are estimated, we use a SIC approach in order to cancel it from the received signal and proceed to the detection of the next target. The procedure stops when no more targets are detected.[5]

At each detection step of the above described procedure, we are in the presence of a binary hypothesis testing where hypotheses $\mathscr{H}_0$ and $\mathscr{H}_1$ correspond to absence or presence of the p-th target only. In fact, when detecting a target and estimating the relevant parameters, the targets already detected are assumed to be already canceled from the received signal whereas the contribution of the remaining targets is assumed to be an additional noise. The observation under the two hypotheses is given by

$$\underline{\mathbf{y}}_b = \begin{cases} \underline{\mathbf{w}}_b & b \in [B] \text{ under } \mathscr{H}_0 \\ \mathring{h}_p\underline{\mathbf{G}}_b(\mathring{\nu}_p, \mathring{\tau}_p, \mathring{\phi}_p)\underline{\mathbf{x}}_b + \underline{\mathbf{w}}_b & b \in [B] \text{ under } \mathscr{H}_1. \end{cases}$$

(14)

In the following, we neglect the arguments in $\underline{\mathbf{G}}_b(\tau_p, \nu_p, \phi_p)$ to avoid excessive clutter in the notation. The log-likelihood ratio for the binary hypothesis testing problem, multiplied by σ_w^2 for convenience, is given by (15), shown at the bottom of the next page.

[5]Alternative stopping criteria can be considered. For example, one may set a limit on the maximum number of targets to be detected at each detection cycle, since this operation is repeated periodically with a certain duty cycle. This depends on the specific application. Note that, in the estimation mode, each acquired user is served via a dedicated RF chain, therefore a limit for the number of detections can be bounded by the number of available RF chains.

Target detection is formulated here as a standard Neyman-Pearson hypothesis testing problem [36], for which the solution that maximizes the detection probability subject to a bound on the false-alarm probability is given by the Likelihood Ratio Test

$$\ell(h_p, \nu_p, \tau_p, \phi_p) \underset{\mathscr{H}_0}{\overset{\mathscr{H}_1}{\gtrless}} T_r, \qquad (16)$$

where the threshold T_r determines the tradeoff between detection and false-alarm probabilities. Since the true value of the parameters is unknown, we use the Generalized Likelihood Ratio Test

$$\max_{h_p, \nu_p, \tau_p, \phi_p} \ell(h_p, \nu_p, \tau_p, \phi_p) \underset{\mathscr{H}_0}{\overset{\mathscr{H}_1}{\gtrless}} T_r. \qquad (17)$$

The maximization of (15) with respect to h_p for fixed τ_p, ν_p, ϕ_p is immediately obtained as

$$\widehat{h}_p = \frac{\left(\sum_{b=1}^{B} \underline{\mathbf{y}}_b^{\mathsf{H}} \underline{\mathbf{G}}_b \underline{\mathbf{x}}_b\right)^*}{\sum_{b=1}^{B} \|\underline{\mathbf{G}}_b \underline{\mathbf{x}}_b\|^2}. \qquad (18)$$

Replacing (18) into (15) we obtain the log-likelihood ratio in the form

$$\ell(\widehat{h}_p, \nu_p, \tau_p, \phi_p) = \frac{\left|\sum_{b=1}^{B} \underline{\mathbf{y}}_b^{\mathsf{H}} \underline{\mathbf{G}}_b \underline{\mathbf{x}}_b\right|^2}{\sum_{b=1}^{B} \|\underline{\mathbf{G}}_b \underline{\mathbf{x}}_b\|^2}. \qquad (19)$$

For future use, we define the function $S(\nu, \tau, \phi)$ given by (19) after replacing $\nu_p \leftarrow \nu, \tau_p \leftarrow \tau, \phi_p \leftarrow \phi$. The proposed successive target detection, parameter estimation, and target signal cancellation works as follows. We define the coarse Doppler-delay-angle search grid $\Gamma \times \widehat{\Omega}$ where Γ is the Doppler-delay grid defined in II-B and $\widehat{\Omega}$ is a suitably defined grid of discrete angles in the designed FoV Ω. The list of detected targets is initialized as "empty". For each detection step $p = 0, 1, 2, \ldots$, the algorithm repeats the following steps:

1) Compute the adaptive threshold function $T_r(\nu, \tau, \phi)$ for all grid points $(\nu, \tau, \phi) \in \Gamma \times \widehat{\Omega}$ according to the Constant False Alarm Rate Detection (CFAR) approach. In particular, here we use the Ordered Statistic Constant False Alarm Rate (OS-CFAR) method, which is known to provide good performance in a realistic scenario when the statistic of noise and interference is not uniformly distributed across the three-dimensional grid (see e.g. [18, Chapter 6.5]). The details of the computation of $T_r(\nu, \tau, \phi)$ are given in Appendix B.
2) Compare $S(\nu, \tau, \phi)$ with the threshold function and define the set of "above threshold" grid points

$$\mathscr{T} = \{(\nu, \tau, \phi) \in \Gamma \times \widehat{\Omega} : S(\nu, \tau, \phi) \geq T_r(\nu, \tau, \phi)\}. \qquad (20)$$

3) If $\mathscr{T} = \emptyset$ (if $\mathscr{T}$ is empty, i.e., $S(\nu, \tau, \phi) < T_r(\nu, \tau, \phi)$ for all grid points), the algorithm exits.

4) If $\mathscr{T} \neq \emptyset$ (and no other stopping criterion is reached), let

$$(\widehat{\nu}_p, \widehat{\tau}_p, \widehat{\phi}_p) = \arg \max_{(\nu, \tau, \phi) \in \mathscr{T}} S(\nu, \tau, \phi), \qquad (21)$$

and declare the new detected p-th target with coarse estimated parameters $(\widehat{\nu}_p, \widehat{\tau}_p, \widehat{\phi}_p)$.
5) Refine the coarse estimate of the parameters over fine grid search localized in the neighborhood of $(\widehat{\nu}_p, \widehat{\tau}_p, \widehat{\phi}_p)$ in the 3-dimensional search space, and let $(\check{\nu}_p, \check{\tau}_p, \check{\phi}_p)$ denote the arg-max of $S(\nu, \tau, \phi)$ on the local search fine grid.
6) Replace $(\check{\nu}_p, \check{\tau}_p, \check{\phi}_p)$ into (18) and find the corresponding estimate $\check{h}_p$ of the channel coefficient. Then, subtract the p-th path signal contribution from the received signal, i.e.,

$$\underline{\mathbf{y}}_b \leftarrow \underline{\mathbf{y}}_b - \check{h}_p \underline{\mathbf{G}}_b(\check{\nu}_p, \check{\tau}_p, \check{\phi}_p) \underline{\mathbf{x}}_b, \quad \text{for } b \in [B].$$

Go back to Step 1 and repeat.

B. Refined Parameter Estimation in Tracking Mode

In Tracking mode, the P users served in spatial division multiple access are chosen by some multiuser MIMO scheduling/grouping scheme (e.g., see [37]) so that they are sufficiently separated in the angle domain thus suffering from very small inter-user interference. It follows that, by design, we have $\mathbf{a}^{\mathsf{H}}(\phi_p)\mathbf{f}_q \approx 0$ for $p \neq q$. From the radar estimation viewpoint, this implies that in this scenario the (known) targets are always clearly distinguishable in the angle domain. Notice that there is no loss of generality in this assumption *precisely* because we are considering the tracking of already connected users, which are scheduled for data transmission and hence chosen (by the multiuser scheduler) to be separable in the angle domain. In other words, if two users are not separable in the angle domain, the BS schedules them in different data frames. This implies that the matrix $\underline{\mathbf{G}}_b(\check{\nu}_p, \check{\tau}_p, \check{\theta}_p)$ defined in (12) can be partitioned into P vertical slices of dimension $N_{\text{rf}}NM \times NM$, where all but the p-th slice are ≈ 0. We define the p-th vertical slice of the channel matrix as

$$\underline{\mathbf{G}}_{b,p}(\mathring{\nu}_p, \mathring{\tau}_p, \mathring{\phi}_p) = \left(\mathbf{U}_b^{\mathsf{H}} \mathbf{a}(\mathring{\phi}_p)\mathbf{a}^{\mathsf{H}}(\mathring{\phi}_p)\mathbf{f}_p\right) \otimes \boldsymbol{\Psi}(\mathring{\nu}_p, \mathring{\tau}_p). \qquad (22)$$

The received signal (13) after neglecting the effect of the almost zero "slices" can be written as

$$\underline{\mathbf{y}}_b \approx \sum_{p=0}^{P-1} \mathring{h}_p \underline{\mathbf{G}}_{b,p}(\mathring{\tau}_p, \mathring{\nu}_p, \mathring{\phi}_p) \underline{\mathbf{x}}_{b,p} + \underline{\mathbf{w}}_b, \quad b \in [B], \qquad (23)$$

where $\underline{\mathbf{x}}_{b,p}$ is the $NM \times 1$ b-th symbol block of the p-th user data stream. We shall develop our ML-based parameter estimation scheme under the assumption that (23) holds with equality. Of course, in simulation, we shall test the scheme with the true channel model given by (13). The excellent performance of the resulting estimator (closely approaching

$$\ell(h_p, \nu_p, \tau_p, \phi_p) = \sigma_w^2 \log \frac{\exp\left(-\frac{1}{\sigma_w^2} \sum_{b=1}^{B} \left\|\underline{\mathbf{y}}_b - h_p \underline{\mathbf{G}}_b \underline{\mathbf{x}}_b\right\|^2\right)}{\exp\left(-\frac{1}{\sigma_w^2} \sum_{b=1}^{B} \|\underline{\mathbf{y}}_b\|^2\right)} = 2\text{Re}\left\{\left(\sum_{b=1}^{B} \underline{\mathbf{y}}_b^{\mathsf{H}} \underline{\mathbf{G}}_b \underline{\mathbf{x}}_b\right) h_p\right\} - |h_p|^2 \sum_{b=1}^{B} \|\underline{\mathbf{G}}_b \underline{\mathbf{x}}_b\|^2 \quad (15)$$

the CRLB) demonstrates the validity of this approximation, which in turns yields a greatly simplified and low complexity estimation scheme.

As before, we neglect the arguments in $\underline{\mathbf{G}}_{b,p}(\tau_p, \nu_p, \phi_p)$. The log-likelihood function, neglecting irrelevant terms, is given by (24), shown at the bottom of the page.

Defining the $P \times 1$ vector of path coefficients $\mathbf{h} = (h_0, \ldots, h_{P-1})^{\mathsf{T}}$, the vector of signal correlations $\mathbf{r}$ with p-th element

$$r_p = \sum_{b=1}^{B} \underline{\mathbf{x}}_{b,p}^{\mathsf{H}} \underline{\mathbf{G}}_{b,p}^{\mathsf{H}} \underline{\mathbf{y}}_b, \qquad (25)$$

the $P \times P$ matrix $\mathbf{A}$ with (p, q) element

$$A_{p,q} = \sum_{b=1}^{B} \underline{\mathbf{x}}_{b,p}^{\mathsf{H}} \underline{\mathbf{G}}_{b,p}^{\mathsf{H}} \underline{\mathbf{G}}_{b,q} \underline{\mathbf{x}}_{b,q}, \qquad (26)$$

and neglecting the irrelevant first term in the RHS of (24), with some abuse of notation, the equivalent log-likelihood function can be written as

$$\Lambda(\{h_p, \nu_p, \tau_p, \phi_p\}) = 2\mathrm{Re}\{\mathbf{h}^{\mathsf{H}}\mathbf{r}\} - \mathbf{h}^{\mathsf{H}}\mathbf{A}\mathbf{h}. \qquad (27)$$

The maximization with respect to $\mathbf{h}$ is readily obtained as $\widehat{\mathbf{h}} = \mathbf{A}^{-1}\mathbf{r}$. Replacing this into (27), the reduced log-likelihood function with respect to the parameters of interest $\{\nu_p, \tau_p, \phi_p\}$ is given by the quadratic form

$$\Lambda_1(\{\nu_p, \tau_p, \phi_p\}) = \mathbf{r}^{\mathsf{H}}\mathbf{A}^{-1}\mathbf{r}. \qquad (28)$$

Notice that (28) must be maximized with respect to the $3P$ parameter variables in order to find the ML parameter estimator. In Tracking mode, the BS has already a coarse knowledge of the parameters of each target (user) since it is transmitting data to them. Therefore, it knows (with some coarse approximation) the AoA (necessary to point the transmit beams), while the delay and Doppler shifts can be obtained (for example) from the data in the uplink. Nevertheless, even with a coarse knowledge of the parameters, a brute-force maximization of (28) is not feasible. For example, a search over a fine grid with 10 points per parameter around their coarse estimates yields already 10^{3P} evaluations of (28). For $P = 3$ this yields 1 billion of points!

This problem is overcome here by noticing a further simplification of the likelihood function. Since the data blocks $\underline{\mathbf{x}}_{b,p}$ are formed by independent zero mean random variables and the block size NM is large, the signal correlation terms $A_{p,q}$ are negligible for $p \neq q$. Neglecting the off-diagonal terms in the matrix $\mathbf{A}$ the reduced log-likelihood function becomes

separable in the individual targets parameters. In fact, it is easily seen that under this simplification we obtain

$$\Lambda_1(\{\nu_p, \tau_p, \phi_p\}) = \sum_{p=0}^{P-1} \frac{\left|\sum_{b=1}^{B} \underline{\mathbf{y}}_b^{\mathsf{H}} \underline{\mathbf{G}}_{b,p} \underline{\mathbf{x}}_{b,p}\right|^2}{\sum_{b=1}^{B} \|\underline{\mathbf{G}}_{b,p} \underline{\mathbf{x}}_{b,p}\|^2}. \qquad (29)$$

Each term in the sum in (29) has a form similar to the function $S(\nu, \tau, \phi)$ defined in (19) and can be maximized individually with respect to the corresponding parameters $\{\nu_p, \tau_p, \phi_p\}$ using the same 3-dimensional grid search as done for the target detection scheme. The numerical results in our simulations are based on this simplified ML-based scheme.

C. Cramér-Rao Lower Bound (CRLB)

We consider the CRLB as a theoretical benchmark, in particular to evaluate the "goodness" of various alternative reduction matrix design (see Remark 1). We consider the case of a single target ($P = N_{\mathrm{s}} = 1$) and drop the index p for simplicity of notation. Letting $A = |h|$ and $\psi = \angle(h)$ denote the amplitude and the phase of h, respectively, five real parameters, denoted by $\boldsymbol{\theta} = (A, \psi, \tau, \nu, \phi)$, shall be estimated. Let $\mathbf{s}_{b,k,l}(\boldsymbol{\theta})$ denote the noise-free received signal at Doppler-delay bin (k, l) and block b, obtained by letting $\mathbf{U} \leftarrow \mathbf{U}_b$ and $P = 1$ in (11). Since the signal is observed in AWGN, we can use the general expression in [38, Sec. 3.9] to obtain the 5×5 Fisher information matrix with (i, j)-th element given by

$$[\mathbf{I}(\mathring{\boldsymbol{\theta}})]_{i,j}$$
$$= \mathrm{Re}\left\{\mathbb{E}\left[\sum_{b=1}^{B} \sum_{k=0}^{N-1} \sum_{l=0}^{M-1} \left(\frac{\partial \mathbf{s}_{b,k,l}(\boldsymbol{\theta})}{\partial \theta_i}\right)^{\mathsf{H}} \left(\frac{\partial \mathbf{s}_{b,k,l}(\boldsymbol{\theta})}{\partial \theta_j}\right)\right]\right\}\Bigg|_{\boldsymbol{\theta}=\mathring{\boldsymbol{\theta}}}, \qquad (30)$$

The complete derivation of the Fisher Information matrix requires straightforward but very cumbersome algebra. The desired CRLB is then obtained by taking the diagonal elements of the inverse Fisher information matrix. The complete derivation of the CRLB is available in an online version of this work [39].

Fig. 2 provides a comparison of the CRLB for different alternative designs of the reduction matrices $\{\mathbf{U}_b\}$ and for the system parameters defined in Table I. This comparison considers three approaches: 1) Proposed method with *Flat-Top* beams. 2) Random selection of N_{rf} antenna elements at each block. 3) A strategy similar to the proposed one, with beams from a DFT grid of beams of size N_{a}. Additionally, as a reference, a fully digital system with $N_{\mathrm{rf}} = N_{\mathrm{a}}$ and $\mathbf{U} = \mathbf{I}_{N_{\mathrm{a}}}$ with only a single integration block is considered. Although this is highly impractical for implementation (as pointed out in Section I), it is provided here as a useful term of comparison.

$$\Lambda(\{h_p, \nu_p, \tau_p, \phi_p\}) = -\sum_{b=1}^{B} \left\|\underline{\mathbf{y}}_b - \sum_{p=0}^{P-1} \underline{\mathbf{G}}_{b,p} \underline{\mathbf{x}}_{b,p}\right\|^2$$
$$= -\sum_{b=1}^{B} \|\underline{\mathbf{y}}_b\|^2 + 2\mathrm{Re}\left\{\sum_{p=0}^{P-1} h_p^* \left(\sum_{b=1}^{B} \underline{\mathbf{x}}_{b,p}^{\mathsf{H}} \underline{\mathbf{G}}_{b,p}^{\mathsf{H}} \underline{\mathbf{y}}_b\right)\right\}$$
$$- \sum_{p=0}^{P-1}\sum_{q=0}^{P-1} h_p^* h_q \left(\sum_{b=1}^{B} \underline{\mathbf{x}}_{b,p}^{\mathsf{H}} \underline{\mathbf{G}}_{b,p}^{\mathsf{H}} \underline{\mathbf{G}}_{b,q} \underline{\mathbf{x}}_{b,q}\right) \qquad (24)$$
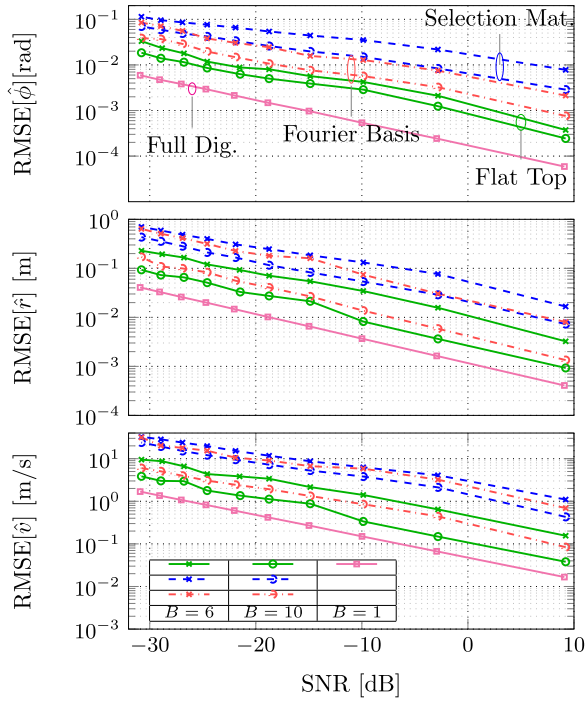
Fig. 2. Comparison of the receive-beamforming strategies over SNR and varying number of integration blocks. SNR values are defined according to (31).

TABLE I
SYSTEM PARAMETERS

$N = 64$	$M = 64$
$f_c = 28.25$ [GHz]	$W = 64$ [MHz]
$P_{\text{avg}} = 24$ [dBm]	$\sigma_{\text{rcs}} = 1$ [m^2]
Noise Figure (NF) $= 2$ [dB]	Noise PSD $N_0 = 2 \cdot 10^{-21}$ [W/Hz]
$N_{\text{a}} = 64$	$N_{\text{rf}} = 4$

V. NUMERICAL RESULTS

A. Simulation Setup

We set the number of RF chains to $N_{\text{rf}} = 4$, such that a single equipment (e.g., BS) is able to jointly track and communicate to N_{rf} distinct targets (or groups of targets), while $N_{\text{rf}} \ll N_{\text{a}}$. A summary of the system parameters is provided in Table I.

The radar two-way pathloss is defined as [18, Chapter 2] PL $= \frac{(4\pi)^3 r^4}{\lambda^2}$, and the resulting SNR at the radar receiver is given by

$$\text{SNR} = \frac{\lambda^2 \sigma_{\text{rcs}}}{(4\pi)^3 r^4} \frac{P_{\text{avg}}}{\sigma_w^2}, \quad (31)$$

where $\lambda = \frac{c}{f_c}$ is the wavelength, c is the speed of light, σ_{rcs} is the radar cross-section of the target in m^2, r is the distance between Tx and Rx, and σ_w^2 is the variance of the AWGN with Power Spectral Density (PSD) of N_0 in W/Hz. We choose $\sigma_{\text{rcs}} = 1$ [m^2] as an indicative value, while different choices for specific cases may be found in literature [40], [41].

Remark 2: In the radar literature, it is customary to consider the resolution limits of each parameter individually. For example, the target (radial) velocity with respect to the

radar receiver is given by $v = \frac{\nu c}{2 f_c}$, and the range (distance between the target and the radar receiver) is given by $r = \frac{\tau c}{2}$. The corresponding velocity, range [42], and approximate angular [22] resolutions, expressed in terms of the system parameters of Table I, are given by

$$v_{\text{res}} = \frac{cW}{2NMf_c} \text{ [m/s]}, \quad r_{\text{res}} = \frac{c}{2W} \text{ [m]},$$

$$\Theta_{\text{res}} = 1.22 \frac{\lambda}{L} \text{ [rad]}, \quad (32)$$

where for the Uniform Linear Array (ULA) described in section II-A, the electrical antenna length L is equal to $\frac{N_{\text{a}}\lambda}{2}$. It can be observed that the velocity and range resolutions are directly proportional to target illumination time (total frame duration) and RF bandwidth, respectively. The single-parameter resolution is (approximately) the minimum spacing such that two targets are distinguishable (i.e., identifiable) in the domain corresponding to the given parameter. At this point, two important observations are in order: 1) in Discovery mode, since the proposed scheme performs a search over the three-dimensional parameter space, two targets become indistinguishable if they are separated by less than the resolution limit in all *three parameters, Doppler, delay,* and *AoA.* For example, two targets may be seen under the same distance and radial velocity, but at different AoA, and yet our scheme with successive detection can detect them with high probability (see for example Fig. 4 marked with †). 2) The resolution limits have little to do with the accuracy (in terms of Mean-Square Error) with which the parameters of detected targets can be estimated in Tracking mode. In fact, our ML-based parameter estimator operates a sort of super-resolution estimation on a much finer search grid, and when not limited by the discretization of the grid, it can approach very closely the CRLB for parameter estimation. ◇

B. Simulation Results

We consider separately the detection performance in Discovery mode and the parameter estimation performance in Tracking mode,

1) Discovery Mode: In this section, we consider the detection probability P_{d} of the proposed method as a function of target range and varying number of integration blocks B for single and multi-target scenarios. Note that range and SNR are related through (31). Given that the initial target acquisition has a direct impact on the latency with which new users can connect to the BS (e.g., during a handover operation), we consider using only relatively small values of $B = \{6, 10, 18\}$. Fig. 3 depicts the simulated scenario for the plots reported in Fig. 4. The plots are obtained by Monte Carlo simulations at each SNR point, where the angles and Doppler shifts of the targets are randomly changed within a wide angular FoV $= [-45°, 45°]$ and radial velocity range $[10 - 60]$ m/s, respectively. More specifically, for the single target scenario in Fig. 3(a), the range parameter takes values in $[10, 20, \ldots, 140]$ [m] and the corresponding P_d is reported in Fig. 4(a).

We consider that a target is correctly detected if the estimated AoA, $\hat{\phi}_p$ fulfills $|\hat{\phi}_p - \phi_p| \leq \epsilon$, with $\epsilon = 0.5°$, since this simulation corresponds to the coarse estimation stage in Discovery mode. We can observe the effect of integration gain on the target detection performance, for which the performance improves with the number of blocks B.
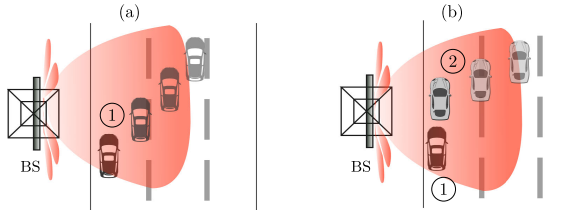
Fig. 3. (a) Movement of a single target inside the considered FoV. (b) Movement scenario of two targets inside the considered FoV, where one target is located at a fixed closer distance and the second changes its position.
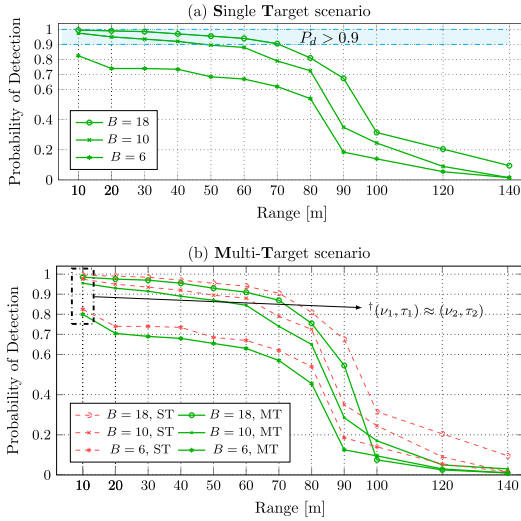

Fig. 4. Probability of detection of targets Vs. range within an illuminated angular FoV of $90°$, as depicted in Fig. 3, with varying B. Plot (a) shows P_d for a single target shown in Fig. 3(a). Plot (b) depicts a two target scenario (Fig. 3(b)) where P_d for the second target after detection and removal of the first target is reported.

Fig. 5. Target positions in Cartesian space.

TABLE II
P_d FOR MULTI-TARGET SCENARIO WITH SIC

Simulation Scenario	Blocks	P_d^{Single}	P_d^{SIC}
Target 1	10	0.96	0.945
Target 2	10	0.935	0.905
Target 3	10	0.895	0.835
Target 4	10	0.84	0.765

Fig. 6. Simulation Scenario in Tracking mode where each of the previously acquired users receives a very narrow signal via a dedicated RF chain.

To demonstrate the effectiveness of the SIC technique of Section IV-A, we consider two distinct experiments. In the first experiment, shown in Fig. 3(b), we consider a two target case, where two targets are present and the detection performance for the second target at different distances is considered while keeping the first target at a fixed short distance. More specifically, one target is located at a close distance of $r = 10$ m, and the second target is located at a distance varying from $r = 10$ m to $r = 140$ m. The closer target creates a masking effect of the second target. By comparing the detection probability P_d versus range in the case of a single target in Fig. 4 (a) with that of the second target in the two-target case in Fig. 4 (b), plotted versus the range of the second target while the first is at fixed short distance, we notice that the proposed SIC scheme is able to cope well with the masked target effect. In fact, P_d for the second target in Fig. 4 (b) is very close to P_d for the single target case in Fig. 4 (a), showing that the presence of a close masking target with strong near-far effect incurs only a small degradation, at least in the relevant range up to 80 m. It should be noted that the effective reliable detection range is a function of transmit power, which can be extended by increasing the transmitter (Tx) power.

In the second experiment, shown in Fig. 5, we consider four targets and repeat the SIC target detection procedure over 200 runs, where the location of each of the targets is shown in Fig. 5. In this experiment, we have considered two
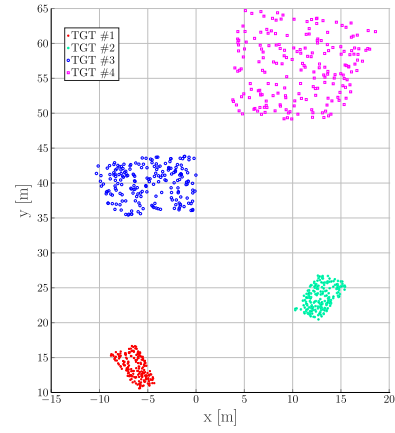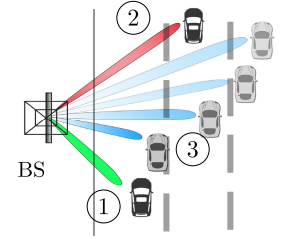
scenarios. In the first scenario, for which the first column of Tab. II, P_d^{Single}, reports the averaged detection probability for the target individually, only a specific single (*isolated*) target is present. The second column, P_d^{SIC}, corresponding to the second scenario, reports the detection probability of each target when all four targets are present at the same time and they are detected sequentially by the SIC procedure. The slight degradation of the detection performance for the farther targets arises from the *residual* of the closer (stronger) targets when their contribution can not be exactly removed.

2) Tracking Mode: Next, the parameter estimation performance of the Tracking mode is considered. Here, the BS sends individually beamformed data streams to P already acquired targets, i.e., *Users*. This results in a significantly higher BF gain of the transmitter and, consequently, a better estimation performance over a wider distance. As shown in Fig. 6, in the simulated scenario three distinct users are considered where the first and second are positioned at a fixed distance and angle from the BS, and the third user's location is changed. Notice that this does not represent relative motion: at each location of the third target, we consider fixed range, Doppler, and AoA for all targets, and perform Monte Carlo simulation of the parameter estimation scheme of Section IV-B. The results are reported in Fig. 7.
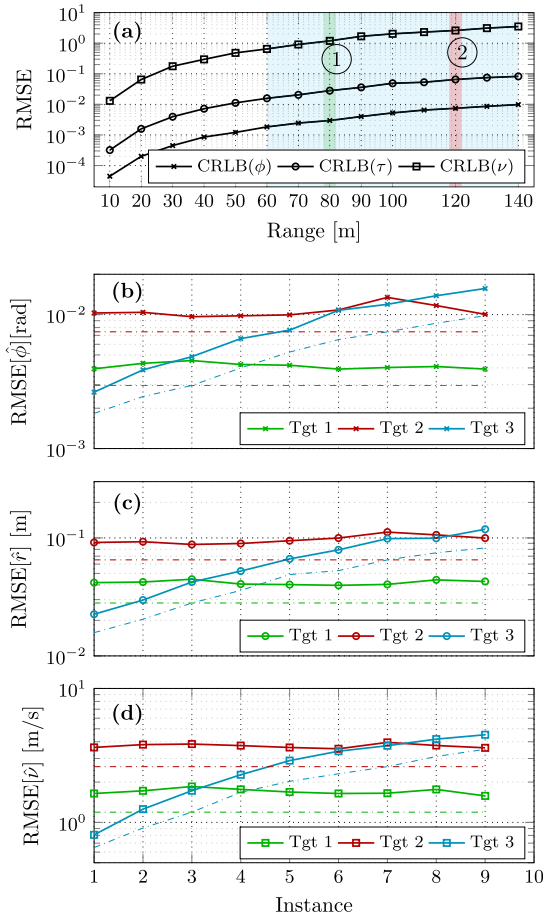
Fig. 7. Estimation performance of Tracking mode. Plot (a) indicates the RMSE values of the three considered parameter estimates as dictated by the CRLB over range (distance). The colored bars indicate the values for the two fixed targets in the setup (see Fig. 6). Plots (b)-(d) depict estimation performance for each target, in AoA, range and radial velocity, respectively.

We compare the achieved root MSE (RMSE) with the corresponding CRLB for all users, indicated by the dashed curves. Interestingly, when two targets have the same range, i.e., location instances 3 and 7, we notice a slight increase in the estimation RMSE. This is because the targets are not distinguishable in the delay domain. However, thanks to their angular separation, the estimation of all the parameters (including the range) remains very accurate. We have also noticed by extensive simulation, that $\mathbf{A}$ in (27) can be safely considered as diagonal, leading to the approximated ML estimator in (29). This is further confirmed by the fact that the performance of the proposed estimator follows closely the CRLB.

Remark 3: We would like to emphasize that the beam-space MIMO approach proposed in this work is not limited to a specific type of beam shape. As an example, when latency is not of concern and therefore a large value of B can be considered, a DFT beamforming dictionary can be used which will increase the SNR at receiver due to higher BF gain. In other applications with relatively narrow FoV requirements, it is possible to replace these flat-top beams or DFT beams with a BF codebook obtained from Slepian sequences, which provide an optimal orthogonality condition and angle concentration around the currently estimated target AOA. This is presented in another related work of ours [15]. ◊

VI. CONCLUSION

In this paper, we proposed a beam-space MIMO radar approach for joint data transmission and radar parameter estimation based on OTFS modulation and targeting mmWave applications. The beam-space approach consists of reducing the N_{a}-dimensional received signal at the radar Rx antenna array to an $N_{\mathrm{rf}} \ll N_{\mathrm{a}}$ projected observation, where the projection is operated by analog BF. In this way, only N_{rf} RF-chains (demodulation and A/D conversion) are needed. We designed a suitable BF codebook and proposed a multi-block detection/estimation scheme, where the projection beam patterns are changed over $B \geq 1$ blocks. We considered two relevant scenarios for joint communication and sensing, namely, Discovery and Tracking modes. In Discovery mode, the BS transmits a wide angle beacon signal and aims to detect known targets (e.g., users entering the cell). In Tracking mode, the BS transmits multiple individually beamformed (with narrow beams) data streams to already acquired users, scheduled to be sufficiently separated in the angle domain.

For Discovery mode, we proposed a sequential target detection with successive interference cancellation, able to cope with the near-far effect yielding target masking in the case of multiple targets. For Tracking mode, we proposed an approximated ML parameter estimator which has relatively low complexity and is able to approach the CRLB on a wide range of the parameters. A few interesting directions are left for future work. These include the further optimization of the hybrid beamforming matrices, the comparison with other radar or/and communication waveforms, and the inclusion of such radar-aided techniques in effective schemes for initial beam acquisition (e.g., radar-enhanced initial beam alignment, for which the Discovery mode is relevant [43]), and in effective schemes for beam tracking (e.g., in conjunction with mobility models and tracking algorithms, for which the Tracking is relevant [44]).

APPENDIX A
DESIGN OF THE BEAMFORMING VECTORS

Let $\mathbf{f}$ be a beamforming vector of dimension N_{a}. Define a discrete set of angles $\Omega = \{\tilde{\phi}_i : i = 1, \ldots, G\}$. The complex-valued (amplitude and phase) beam pattern radiated by the array at each sampling point $\tilde{\phi}_i$ is given by the inner product of $\mathbf{f}$ and the array response vector $\mathbf{a}(\phi)$ at the given grid angle, i.e., $\mathbf{a}^{\mathsf{H}}(\tilde{\phi}_i)\mathbf{f}$.

The design problem of interest is to find $\mathbf{f}$ to approach a desired radiation pattern $\bar{\mathbf{b}} \in \mathbb{R}^G$, where the entries of $\bar{\mathbf{b}} = [\bar{b}_1, \ldots, \bar{b}_G]^{\mathsf{T}}$ are the magnitudes of the radiation pattern at the discrete angles in Ω. In particular, we fix $\bar{\mathbf{b}}$ to have a constant level in a pre-determined angle range around the boresight direction of the array (zero angle) and such that the values corresponding to the rejection directions (sidelobes) are below a certain threshold with respect to the maximum (center beam). By letting $\mathbf{A} = [\mathbf{a}(\tilde{\phi}_1), \ldots, \mathbf{a}(\tilde{\phi}_G)]$, this problem can be formulated as a magnitude least-squares problem which belongs to the class of problems addressed by [45] and [46].

$$\min_{\mathbf{f}} \ \|\mathbf{A}^{\mathsf{H}}\mathbf{f} - \bar{\mathbf{b}}\|^2$$
$$\text{s.t. } \mathbf{f}^{\mathsf{H}}\mathbf{A}^{\mathsf{H}}\mathbf{A}\mathbf{f} = 1 \qquad (33)$$

where the constraint in (33) imposes unit transmit power. Problem (33) can be solved as a semidefinite relaxation of the magnitude least-squares problem [46]. Depending on the
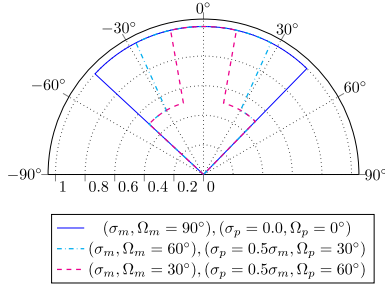
Fig. 8. Examples of beampattern masks with varying main lobe widths and sidelobe levels.
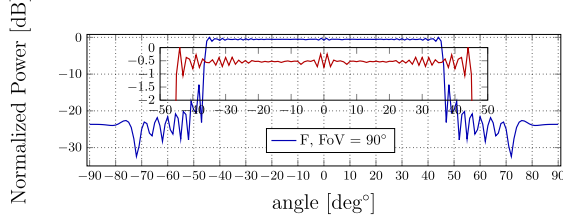

Fig. 9. Tx beampattern for a FoV of $90°$ and $N_a = 64$. The zoomed-in plot depicts the minimal ripple within the main beam.

operating scenario, a beam pattern can focus the transmitted energy on an angular sector of given width in the FoV defined by Ω. In order to define our design in a flexible manner, the FoV is divided into a central section Ω_m covering G_m discrete directions each with magnitude of σ_m and the remaining sections (modulo the interval $[-\pi, \pi]$ denoted by Ω_p, with G_p grid points and magnitude σ_p). The desired beam pattern $\mathbf{b}$ has a total power of $G_m\sigma_m^2$ in the central sector and $G_p\sigma_p^2 = 1 - G_m\sigma_m^2$ in the remaining peripheral sections. By controlling the main and peripheral sections, we can control the width of the main lobe and the side lobes rejection.

Fig. 8 shows a few examples of the used design beamforming masks. Fig. 9 illustrates the achieved flat-top beampattern for an FoV of $90°$, corresponding to the wide Tx beam used in Discovery mode in this paper.

APPENDIX B
ADAPTIVE THRESHOLD FOR DETECTION

With reference to the notation introduced in Section IV-A, the decision statistics at each Doppler-delay-angle bin $(\nu, \tau, \phi) \in \Gamma \times \widehat{\Omega}$ under hypothesis $\mathscr{H}_0$ if given by

$$S^{\mathscr{H}_0}(\nu, \tau, \phi) := \frac{\left|\sum_{b=1}^{B} \underline{\mathbf{w}}_b^{\mathsf{H}} \underline{\mathbf{G}}_b(\nu, \tau, \phi)\underline{\mathbf{x}}_b\right|^2}{\sum_{b=1}^{B} \|\underline{\mathbf{G}}_b(\nu, \tau, \phi)\underline{\mathbf{x}}_b\|^2},$$

$$S^{\mathscr{H}_1}(\nu, \tau, \phi) := \frac{\left|\sum_{b=1}^{B} \underline{\mathbf{y}}_b^{\mathsf{H}} \underline{\mathbf{G}}_b(\nu, \tau, \phi)\underline{\mathbf{x}}_b\right|^2}{\sum_{b=1}^{B} \|\underline{\mathbf{G}}_b(\nu, \tau, \phi)\underline{\mathbf{x}}_b\|^2}. \quad (34)$$

We wish to compute an adaptive thresholds $T_r(\nu, \tau, \phi)$ to compare the decision statistic $S(\nu, \tau, \phi)$ and decide for $\mathscr{H}_0$ or $\mathscr{H}_1$, such that a target false alarm probability is achieved.

Notice that the function $S^{\mathscr{H}_0}(\nu, \tau, \phi)$ is the squared magnitude of a Gaussian complex circularly symmetric random variable obtained as the linear projection of the AWGN vector. Hence, it is exponentially distributed (for given $\{\underline{\mathbf{G}}_b(\nu, \tau, \phi)\underline{\mathbf{x}}_b\}_{b=1}^{B}$).
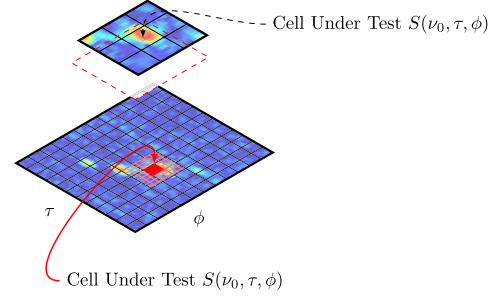

Fig. 10. Graphical representation of OS-CFAR windowing. For a plane cut at $\nu = \nu_0$, the window is shifted around each location (ν_0, τ, ϕ) in the search space.

We can estimate the distribution locally at each Doppler-delay-angle bin $(\nu, \tau, \phi) \in \Gamma \times \widehat{\Omega}$. Following the OS-Constant False Alarm Rate (CFAR) procedure [18, Chapter 6.5], we first define a set of neighboring bins, denoted by $\mathscr{C}(\nu, \tau, \phi)$, centered at (ν, τ, ϕ) (see Fig. 10). Let $N_c = \max_{(\nu, \tau, \phi) \in \Gamma \times \widehat{\Omega}} |\mathscr{C}(\nu, \tau, \phi)|$ denote the size of the neighboring bins for most of bins in the search space (notice that for some bins in the boundary of the domain the size of the neighboring set $\mathscr{C}(\nu, \tau, \phi)$ may be less than N_c). For each Doppler-delay-angle bin $(\nu, \tau, \phi) \in \Gamma \times \widehat{\Omega}$, we evaluate the value of $S(\nu', \tau', \phi')$ for $(\nu', \tau', \phi') \in \mathscr{C}(\nu, \tau, \phi)$ and sort them in an increasing order such that

$$S(\nu_1, \tau_1, \phi_1) \leq S(\nu_2, \tau_2, \phi_2) \leq \cdots \leq S(\nu_{N_c}, \tau_{N_c}, \phi_{N_c}) \quad (35)$$

where $(\nu_i, \tau_i, \phi_i) \in \mathscr{C}(\nu, \tau, \phi)$ denotes the i-th element in the above ordered statistics of the neighboring set. Assuming that no target falls in the neighboring set $\mathscr{C}(\nu, \tau, \phi)$, the above ordered statistics yields an empirical cumulative distribution function (CDF) of $S(\nu, \tau, \phi)$. Hence, the threshold can be determined by choosing a given percentile κ of this empirical CDF, and scaling it by a factor α that depends on the specific problem at hand and must be tuned through simulations. Specifically, fixing $\kappa \in (0, 1)$, we express the adaptive threshold $T_r(\nu, \tau, \phi)$ as

$$T_r(\nu, \tau, \phi) = \alpha S(\nu_{\lceil \kappa N_c \rceil}, \tau_{\lceil \kappa N_c \rceil}, \phi_{\lceil \kappa N_c \rceil}). \quad (36)$$

The corresponding false alarm probability at bin (ν, τ, ϕ) if given by

$$P_{\mathrm{fa}}(\nu, \tau, \phi) = \mathbb{P}(S(\nu, \tau, \phi) > T_r(\nu, \tau, \phi)|\mathscr{H}_0)$$
$$\approx 1 - \hat{F}_{S^{\mathscr{H}_0}}(T_r(\nu, \tau, \phi)) \quad (37)$$

where $\hat{F}_{S^{\mathscr{H}_0}}$ denotes the empirical CDF of $S^{\mathscr{H}_0}(\nu, \tau, \phi)$ calculated from the ordered statistics defined above. The average false alarm probability is given by

$$\bar{P}_{\mathrm{fa}} = \frac{1}{|\Gamma||\widehat{\Omega}|} \sum_{(\nu, \tau, \phi) \in \Gamma \times \widehat{\Omega}} P_{\mathrm{fa}}(\nu, \tau, \phi) \quad (38)$$

and depends on κ and α. Then, we can tune these parameters such that a target average false alarm probability is satisfied. This is obtained by simulation (in our case) or by training (in a real-world scenario).

Fig. 11 shows the three stages of the OS-CFAR procedure in a 2-dimensional *delay-angle* space (a depiction in 2-D space is shown for visualization clarity). Fig. 11 (a) shows
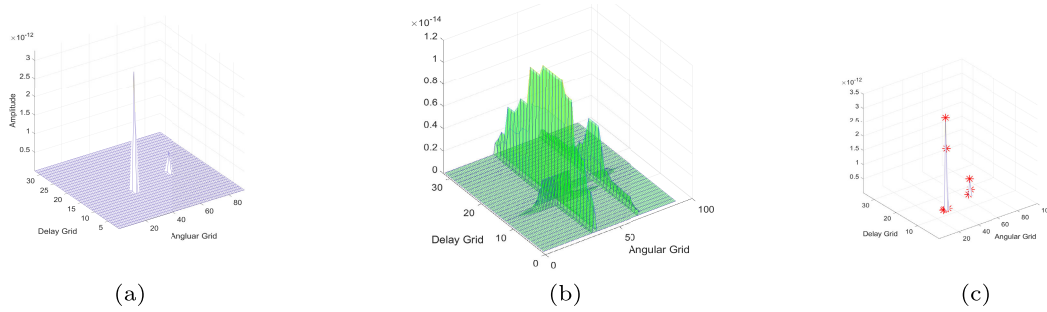
Fig. 11. Illustrative description of the three stages of the OS-CFAR procedure, namely, (a) received signal as input, (b) calculating the threshold and, (c) applying the threshold against the signal to obtain detections.

the decision statistics $S(\nu, \tau, \phi)$ for $\nu = 0$, in the delay-angle plane. Fig. 11 (b) shows the threshold $T_r(\nu, \tau, \phi)$ calculated according to the above OS-CFAR procedure. Fig. 11 (c) shows the portion of the detection statistics in (a) above the adaptive threshold in (b). This determines the set of points in the grid above threshold $\mathscr{T}$ as defined in (20). Finally, the target is identified by taking the position of the maximum of $S(\nu, \tau, \phi)$ for over the set $\mathscr{T}$, if this is not empty, otherwise hypothesis $\mathscr{H}_0$ (no target) is declared.

REFERENCES

[1] A. N. Uwaechia and N. M. Mahyuddin, "A comprehensive survey on millimeter wave communications for fifth-generation wireless networks: Feasibility and challenges," *IEEE Access*, vol. 8, pp. 62367–62414, 2020.

[2] X. Song, T. Kuhne, and G. Caire, "Fully-/partially-connected hybrid beamforming architectures for mmWave MU-MIMO," *IEEE Trans. Wireless Commun.*, vol. 19, no. 3, pp. 1754–1769, Mar. 2020.

[3] X. Song, S. Haghighatshoar, and G. Caire, "A scalable and statistically robust beam alignment technique for millimeter-wave systems," *IEEE Trans. Wireless Commun.*, vol. 17, no. 7, pp. 4792–4805, Jul. 2018.

[4] W. Yuan, F. Liu, C. Masouros, J. Yuan, D. W. K. Ng, and N. González-Prelcic, "Bayesian predictive beamforming for vehicular networks: A low-overhead joint radar-communication approach," *IEEE Trans. Wireless Commun.*, vol. 20, no. 3, pp. 1442–1456, Mar. 2021.

[5] Z. Du et al., "Integrated sensing and communications for V2I networks: Dynamic predictive beamforming for extended vehicle targets," *IEEE Trans. Wireless Commun.*, early access, Nov. 11, 2021, doi: 10.1109/TWC.2022.3219890.

[6] S. K. Dehkordi, M. Kobayashi, and G. Caire, "Adaptive beam tracking based on recurrent neural networks for mmWave channels," in *Proc. IEEE 22nd Int. Workshop Signal Process. Adv. Wireless Commun. (SPAWC)*, Sep. 2021, pp. 1–5.

[7] S. H. Dokhanchi, B. S. Mysore, K. V. Mishra, and B. Ottersten, "A mmWave automotive joint radar-communications system," *IEEE Trans. Aerosp. Electron. Syst.*, vol. 55, no. 3, pp. 1241–1260, Jun. 2019.

[8] L. Zheng, M. Lops, Y. C. Eldar, and X. Wang, "Radar and communication coexistence: An overview: A review of recent methods," *IEEE Signal Process. Mag.*, vol. 36, no. 5, pp. 85–99, Sep. 2019.

[9] A. Hassanien, M. G. Amin, E. Aboutanios, and B. Himed, "Dual-function radar communication systems: A solution to the spectrum congestion problem," *IEEE Signal Process. Mag.*, vol. 36, no. 5, pp. 115–126, Sep. 2019.

[10] L. Gaudio, M. Kobayashi, G. Caire, and G. Colavolpe, "On the effectiveness of OTFS for joint radar parameter estimation and communication," *IEEE Trans. Wireless Commun.*, vol. 19, no. 9, pp. 5951–5965, Sep. 2020.

[11] R. Hadani et al., "Orthogonal time frequency space modulation," in *Proc. IEEE Wireless Commun. Network. Conf. (WCNC)*, Mar. 2017, pp. 1–6.

[12] W. Shen, L. Dai, J. An, P. Fan, and R. W. Heath Jr., "Channel estimation for orthogonal time frequency space (OTFS) massive MIMO," *IEEE Trans. Signal Process.*, vol. 67, no. 16, pp. 4204–4217, Aug. 2019.

[13] M. K. Ramachandran and A. Chockalingam, "MIMO-OTFS in high-Doppler fading channels: Signal detection and channel estimation," in *Proc. IEEE Global Commun. Conf. (GLOBECOM)*, Dec. 2018, pp. 206–212.

[14] L. Gaudio, G. Colavolpe, and G. Caire, "OTFS vs. OFDM in the presence of sparsity: A fair comparison," *IEEE Trans. Wireless Commun.*, vol. 21, no. 6, pp. 4410–4423, Jun. 2022.

[15] F. Pedraza, M. Kobayashi, and G. Caire, "Beam refinement and user state acquisition via integrated sensing and communication with OFDM," in *Proc. IEEE 22nd Int. Workshop Signal Process. Adv. Wireless Commun. (SPAWC)*, Sep. 2021, pp. 476–480.

[16] S. M. Patole, M. Torlak, D. Wang, and M. Ali, "Automotive radars: A review of signal processing techniques," *IEEE Signal Process. Mag.*, vol. 34, no. 2, pp. 22–35, Mar. 2017.

[17] J. Li and P. Stoica, *MIMO Radar Signal Processing*. Hoboken, NJ, USA: Wiley, 2008.

[18] M. A. Richards, *Fundamentals of Radar Signal Processing*, 2nd ed. New York, NY, USA: McGraw-Hill, 2014.

[19] D. K. Pin Tan et al., "Integrated sensing and communication in 6G: Motivations, use cases, requirements, challenges and future directions," in *Proc. 1st IEEE Int. Online Symp. Joint Commun. Sens.*, Feb. 2021, pp. 1–6.

[20] F. Liu et al., "Integrated sensing and communications: Toward dual-functional wireless networks for 6G and beyond," *IEEE J. Sel. Areas Commun.*, vol. 40, no. 6, pp. 1728–1767, Jun. 2022.

[21] Z. Chen, Z. Cao, X. He, Y. Jin, J. Li, and P. Chen, "DoA and DoD estimation and hybrid beamforming for radar-aided mmWave MIMO vehicular communication systems," *Electronics*, vol. 7, no. 3, p. 40, Mar. 2018.

[22] J. Hatch, A. Topak, R. Schnabel, T. Zwick, R. Weigel, and C. Waldschmidt, "Millimeter-wave technology for automotive radar sensors in the 77 GHz frequency band," *IEEE Trans. Microw. Theory Techn.*, vol. 60, no. 3, pp. 845–860, Mar. 2012.

[23] H. Wymeersch et al., "6G radio requirements to support integrated communication, localization, and sensing," 2022, *arXiv:2205.10783*.

[24] H. L. V. Trees, *Optimum Array Processing: Part IV of Detection, Estimation, and Modulation Theory*. Hoboken, NJ, USA: Wiley, 2002.

[25] R. Rotman, M. Tur, and L. Yaron, "True time delay in phased arrays," *Proc. IEEE*, vol. 104, no. 3, pp. 504–518, Mar. 2016.

[26] A. Sabharwal, P. Schniter, D. Guo, D. W. Bliss, S. Rangarajan, and R. Wichman, "In-band full-duplex wireless: Challenges and opportunities," *IEEE J. Sel. Areas Commun.*, vol. 32, no. 9, pp. 1637–1652, Sep. 2014.

[27] S. M. Wentworth, *Applied Electromagnetics: Early Transmission Lines Approach*. Hoboken, NJ, USA: Wiley, 2007.

[28] M. Duarte and A. Sabharwal, "Full-duplex wireless communications using off-the-shelf radios: Feasibility and first results," in *Proc. 44th Asilomar Conf. Signals, Syst. Comput.*, Nov. 2010, pp. 1558–1562.

[29] P. Kumari, J. Choi, N. González-Prelcic, and R. W. Heath, "IEEE 802.11ad-based radar: An approach to joint vehicular communication-radar system," *IEEE Trans. Veh. Technol.*, vol. 67, no. 4, pp. 3012–3027, Apr. 2018.

[30] D. H. N. Nguyen and R. W. Heath Jr., "Delay and Doppler processing for multi-target detection with IEEE 802.11 OFDM signaling," in *Proc. IEEE Int. Conf. Acoust., Speech Signal Process. (ICASSP)*, New Orleans, LA, USA, Mar. 2017, pp. 3414–3418.

[31] E. Grossi, M. Lops, L. Venturino, and A. Zappone, "Opportunistic radar in IEEE 802.11ad networks," *IEEE Trans. Signal Process.*, vol. 66, no. 9, pp. 2441–2454, Mar. 2018.

[32] G. A. Vitetta, D. P. Taylor, G. Colavolpe, F. Pancaldi, and P. A. Martin, *Wireless Communications: Algorithmic Techniques*. Hoboken, NJ, USA: Wiley, 2013.

[33] P. Raviteja, K. T. Phan, Y. Hong, and E. Viterbo, "Interference cancellation and iterative detection for orthogonal time frequency space modulation," *IEEE Trans. Wireless Commun.*, vol. 17, no. 10, pp. 6501–6515, Oct. 2018.

[34] F. Sohrabi and W. Yu, "Hybrid digital and analog beamforming design for large-scale antenna arrays," *IEEE J. Sel. Topics Signal Process.*, vol. 10, no. 3, pp. 501–513, Apr. 2016.

[35] G. Matz, H. Bolcskei, and F. Hlawatsch, "Time-frequency foundations of communications: Concepts and tools," *IEEE Signal Process. Mag.*, vol. 30, no. 6, pp. 87–96, Jun. 2013.

[36] H. V. Poor, *An Introduction to Signal Detection and Estimation*. 2nd ed. Berlin, Germany: Springer-Verlag, 1994.

[37] J. Nam, A. Adhikary, J.-Y. Ahn, and G. Caire, "Joint spatial division and multiplexing: Opportunistic beamforming, user grouping and simplified downlink scheduling," *IEEE J. Sel. Topics Signal Process.*, vol. 8, no. 5, pp. 876–890, Oct. 2014.

[38] S. M. Kay, *Fundamentals of Statistical Signal Processing: Estimation Theory*. Upper Saddle River, NJ, USA: Prentice-Hall, 1993.

[39] S. K. Dehkordi, L. Gaudio, M. Kobayashi, G. Caire, and G. Colavolpe, "Beam-space MIMO radar for joint communication and sensing with OTFS modulation," 2022, *arXiv:2207.05337*.

[40] H. Suzuki, "Measurement results of radar cross section of automobiles for millimeter wave band," in *Proc. 7th World Congr. Intell. Syst.*, 2000, pp. 2445–2449.

[41] E. B. Kamel, A. Peden, and P. Pajusco, "RCS modeling and measurements for automotive radar applications in the W band," in *Proc. 11th Eur. Conf. Antennas Propag. (EUCAP)*, Mar. 2017, pp. 2445–2449.

[42] Y. Liu, G. Liao, Y. Chen, J. Xu, and Y. Yin, "Super-resolution range and velocity estimations with OFDM integrated radar and communications waveform," *IEEE Trans. Veh. Technol.*, vol. 69, no. 10, pp. 11659–11672, Oct. 2020.

[43] M. A. Islam, G. C. Alexandropoulos, and B. Smida, "Integrated sensing and communication with millimeter wave full duplex hybrid beamforming," 2022, *arXiv:2201.05240*.

[44] F. Pedraza, S. K. Dehkordi, M. Kobayashi, and G. Caire, "Simultaneous communication and tracking in arbitrary trajectories via beam-space processing," 2022, *arXiv:2203.15420*.

[45] M. Goemans and D. Williamson, "Improved approximation algorithms for maximum cut and satisfiability problems using semidefinite programming," *J. Assoc. Comput. Machinery*, vol. 42, no. 6, pp. 1115–1145, 1995.

[46] P. W. Kassakian, "Convex approximation and optimization with applications in magnitude filter design and radiation pattern synthesis," Ph.D. dissertation, Univ. California, Berkeley, Berkeley, CA, USA, 2006.

Saeid K. Dehkordi (Graduate Student Member, IEEE) is currently pursuing the Ph.D. degree with the Faculty of Electrical Engineering and Computer Science, Technical University of Berlin, Germany. He worked at Daimler AG and APTIV in the field of automotive radar perception as a Research Engineer. His main research interests are in the field of signal processing with a particular focus on wireless communications.

Lorenzo Gaudio received the Master of Science degree (cum laude) in communication engineering from the University of Parma, Parma, Italy, in 2017, and the Ph.D. degree in information technology from the Department of Engineering and Architecture, University of Parma, in 2021. His main research interests include digital communications systems, channel coding and information theory, and signal processing.

Mari Kobayashi (Senior Member, IEEE) received the B.E. degree in electrical engineering from Keio University, Yokohama, Japan, in 1999, and the M.S. and Ph.D. degrees in mobile radio from the École Nationale Supérieure des Télécommunications, Paris, France, in 2000 and 2005, respectively. From November 2005 to March 2007, she was a Post-Doctoral Researcher with the Centre Tecnològic de Telecomunicacions de Catalunya, Barcelona, Spain. In May 2007, she joined the Telecommunications Department, Centrale Supélec, Gif-sur-Yvette, France, where she is currently a Professor. She was an Alexander von Humboldt Experienced Research Fellow (September 2017–April 2019) and an August-Wihelm Scheer Visiting Professor (August 2019–April 2020) at the Technical University of Munich (TUM). She was a recipient of the Newcom++ Best Paper Award in 2010, the IEEE Comsoc/IT Joint Society Paper Award in 2011, and the ICC Best Paper Award in 2019.

Giuseppe Caire (Fellow, IEEE) was born in Torino in 1965. He received the B.Sc. degree in electrical engineering from the Politecnico di Torino in 1990, the M.Sc. degree in electrical engineering from Princeton University in 1992, and the Ph.D. degree from the Politecnico di Torino in 1994.

He was a Post-Doctoral Research Fellow with the European Space Agency (ESTEC), Noordwijk, The Netherlands, from 1994 to 1995; an Assistant Professor of telecommunications with the Politecnico di Torino; an Associate Professor with the University of Parma, Italy; a Professor with the Department of Mobile Communications, Eurecom Institute, Sophia-Antipolis, France; and a Professor of electrical engineering with the Viterbi School of Engineering, University of Southern California, Los Angeles. He is currently an Alexander von Humboldt Professor with the Faculty of Electrical Engineering and Computer Science, Technical University of Berlin, Germany. His main research interests are in the field of communications theory, information theory, and channel and source coding, with a particular focus on wireless communications. He was a recipient of the 2021 Leibniz Prize of the German National Science Foundation (DFG). He has served in the Board of Governors for the IEEE Information Theory Society from 2004 to 2007 and an Officer from 2008 to 2013. He received the Jack Neubauer Best System Paper Award from the IEEE Vehicular Technology Society in 2003, the IEEE Communications Society and Information Theory Society Joint Paper Award in 2004 and 2011, the Okawa Research Award in 2006, the Alexander von Humboldt Professorship in 2014, the Vodafone Innovation Prize in 2015, an ERC Advanced Grant in 2018, the Leonard G. Abraham Prize for Best IEEE JOURNAL ON SELECTED AREAS IN COMMUNICATIONS Paper in 2019, and the IEEE Communications Society Edwin Howard Armstrong Achievement Award in 2020. He was the President of the IEEE Information Theory Society in 2011.

Giulio Colavolpe (Senior Member, IEEE) received the Dr.-Ing. degree (cum laude) in telecommunications engineering from the University of Pisa, Italy, in 1994, and the Ph.D. degree in information technologies from the University of Parma, Italy, in 1998. Since 1997, he has been with the University of Parma, where he is currently a Professor of telecommunications with the Dipartimento di Ingegneria e Architettura (DIA). In 2000, he was a Visiting Scientist with the Institut Eurécom, Valbonne, France. In 2013, he was a Visiting Scientist with the European Space Agency (ESTEC), Noordwijk, The Netherlands. His research activity has led to more than 200 papers in refereed journals and in leading international conferences, and 18 industrial patents. His research interests include the design of digital communication systems, adaptive signal processing (with particular emphasis on iterative detection techniques for channels with memory), and channel coding and information theory. He received the Best Paper Award at the 13th International Conference on Software, Telecommunications and Computer Networks (SoftCOM 2005), Split, Croatia, in September 2005; the Best Paper Award for Optical Networks and Systems at the IEEE International Conference on Communications (ICC 2008), Beijing, China, in May 2008; and the Best Paper Award at the Fifth Advanced Satellite Mobile Systems Conference and the 11th International Workshop on Signal Processing for Space Communications (ASMS&SPSC 2010), Cagliari, Italy. He served as an Editor for the IEEE TRANSACTIONS ON WIRELESS COMMUNICATIONS, the IEEE TRANSACTIONS ON COMMUNICATIONS, and the IEEE WIRELESS COMMUNICATIONS LETTERS; and an Executive Editor for *Transactions on Emerging Telecommunications Technologies* (ETT).